Weierstraß-Institut
für Angewandte Analysis und Stochastik
Leibniz-Institut im Forschungsverbund Berlin e. V.

Preprint ISSN 0946 – 8633

Amplifications of picosecond laser pulses in tapered semiconductor amplifiers: Numerical simulations versus experiments

Vasile Tronciu [1], Sven Schwertfeger [2], Mindaugas Radziunas [1],

Andreas Klehr [2], Uwe Bandelow [1], Hans Wenzel [2]

submitted: October 26, 2011

[1] Weierstrass Institute
Mohrenstrasse 39
10117 Berlin
Germany
E-Mail: vasile.tronciu@wias-berlin.de
E-Mail: mindaugas.radziunas@wias-berlin.de
E-Mail: uwe.bandelow@wias-berlin.de

[2] Ferdinand-Braun-Institut für
Höchstfrequenztechnik
Gustav-Kirchhoff-Str. 4
12489 Berlin
Germany
E-Mail: wenzel@fbh-berlin.de

No. 1657
Berlin 2011

2010 *Mathematics Subject Classification.* 78A60 37M05.

2008 *Physics and Astronomy Classification Scheme.* 42.60.Da, 42.60.Jf.

Key words and phrases. picosecond pulse amplification, tapered semiconductor amplifier.

This work was supported by the German Ministry for Education and Research (BMBF) within the project “INDILAS” (contract FKZ 13N9816). The authors thank M. Lichtner for fruitful collaboration. V.Z.T. acknowledges R.A. Abram for discussions. The work of M.R. and U.B. was also supported by DFG Research Center MATHEON “Mathematics for key technologies: Modelling, simulation and optimization of the real world processes”.

Edited by
Weierstraß-Institut für Angewandte Analysis und Stochastik (WIAS)
Leibniz-Institut im Forschungsverbund Berlin e. V.
Mohrenstraße 39
10117 Berlin
Germany

Fax: +49 30 2044975
E-Mail: preprint@wias-berlin.de
World Wide Web: http://www.wias-berlin.de/

Abstract

We apply a travelling wave model to the simulation of the amplification of laser pulses generated by Q-switched or mode-locked distributed-Bragg reflector lasers. The power amplifier monolithically integrates a ridge-waveguide section acting as pre-amplifier and a flared gain-region amplifier. The diffraction limited and spectral-narrow band pulses injected in to the pre-amplifier have durations between 10 ps and 100 ps and a peak power of typical 1 W. After the amplifier, the pulses reach a peak power of several tens of Watts preserving the spatial, spectral and temporal properties of the input pulse. We report results obtained by a numerical solution of the travelling-wave equations and compare them with experimental investigations. The peak powers obtained experimentally are in good agreement with the theoretical predictions. The performance of the power amplifier is evaluated by considering the dependence of the pulse energy as a function of different device and material parameters.

1 Introduction

During recent years, picosecond laser sources have found many applications in fields such as material processing, remote sensing, and fluorescence spectroscopy [1–3]. Optical pulses in the picosecond range can be generated with diode lasers by mode-locking, Q-switching, and gain switching [4]. The pulse energies of several hundreds of pJ and peak powers up to 1 W emitted from these diode lasers are often not sufficient for many applications.

Higher pulse energies can be obtained by amplification of the pulses with master-oscillator power-amplifier (MOPA) systems [3], [5]-[10]. Mostly the power amplifier is operated in continuous-wave mode. This leads to the generation of amplified spontaneous emission (ASE) [8], [10]. Especially if the amplifier is seeded with optical pulses with repetition rates in the MHz range most of the emitted power consists of ASE.

In a recent paper [5], an experimental setup was presented where the power amplifier is driven with short electrical pulses of high amplitude to reduce the ASE between the pulses independently from the repetition frequency. Short optical pulses with a high peak power of 50 W and a pulse energy larger than 4 nJ were obtained. These values exceeded the values

presented in [6], [8]-[10] for single-stage semiconductor based setups like in [5]. Compared to some two-stage setups [3], [7], higher pulse energies with less complexity of the experimental assembly were reached. Most of the experimental work mentioned above including [5] lack a comparison with theoretical results.

Different theoretical models for studying the propagation of picosecond pulses in optical amplifiers have been proposed in the literature. A microscopic model based on spatially resolved Maxwell–Bloch–Langevin equations taking into account many-body interactions, energy transfer between the carrier and phonon systems and the spatio–temporal interplay of stimulated and amplified spontaneous emission was presented in [11]. Although it was applied to the investigation of various short tapered semiconductor optical amplifiers for picosecond pulse amplification, due to the extremely large numerical effort a computation of input-output characteristics and a systematic parameter study was not carried out.

A time domain model based on the travelling wave equations for the simulation of the picosecond pulse amplification in flared amplifiers was presented in [12] and [13]. The model includes the effects of gain saturation, finite-gain bandwidth, self-phase modulation, index dispersion, carrier heating, carrier diffusion and recombination and is capable to investigate the propagation of sub-picosecond pulses. However, a comparison with experimental results was not given.

An analysis of the amplification characteristics of picosecond Gaussian pulses in non-tapered and tapered amplifiers was performed in [14] based on a numerical solution of rate equations. It has been shown that in contrast to the conventional non-tapered amplifiers, the tapered structure can provide nearly distortionless amplification for input pulses with high energy levels. However, effects like diffraction and self-focusing can not be handled by the model due to the simplifications involved.

Analytical solutions and a systematic way to construct approximate solutions for the gain-recovery dynamics of semiconductor optical amplifiers were given in [15]. The analytical results show excellent agreement with those obtained numerically.

The purpose of the present paper is to investigate both theoretically and experimentally the characteristics of the amplification of picosecond pulses in tapered amplifiers and to determine the parameters and geometrical design of the amplifier for optimum performance.

The paper is structured as follows. The device structure and mathematical model are presented in Section 2. The pulse propagation within the device is described in Section 3. In Section 4 we present results obtained by numerical simulations based on the travelling wave model and compare them with experimental data. Section 5 deals with the influence of material and device parameters on the pulse propagation. We summarize the main results of the paper in Section 6.

2. Experimental setup and theoretical model

The experimental setup is shown schematically in Fig. 1. Optical pulses generated by Q-switching of a three-section distributed Bragg reflector (DBR) laser acting as master oscillator (MO) are injected into a two-section tapered semiconductor power amplifier (PA).

The DBR laser consists of an active gain section, a saturable absorber section (SAB) and a DBR section as described in [5]. The lengths of the sections are L_{gain} = 1 mm, L_{SAB} = 0.5 mm and L_{DBR} = 0.5 mm. The laser has a ridge waveguide (RW) for lateral optical confinement with a ridge width of 5 µm. The vertical layer structure consists of an active region with two InGaAs quantum wells (QWs) extending over all sections and an AlGaAs based waveguide with a core width of 4.8 µm. The second order Bragg grating with a period of 329 nm has a coupling coefficient of about 40 cm^{-1} leading to an effective reflectivity of the Bragg grating of R_{DBR}~90% with a spectral width of 0.7 nm.
Q-switching is realized by injecting short electrical pulses into the SAB section of the three-section DBR laser so that this section becomes optically transparent. These pulses are generated with an Agilent 81134A pulse pattern generator and amplified with an emitter coupled logic (ECL) based electrical circuit developed in-house. The current pulse amplitude is about 500 mA and the pulse full width at half maximum (FWHM) is 730 ps. The repetition rate is 20 MHz.
The tapered PA consists of a 1 mm long index-guided preamplifier (PRE) and a 3 or 5 mm long gain-guided tapered power amplifier (TAP). The PRE section having a RW with a ridge width of 5 µm acts like a mode filter and shapes the optical pulse, whereas the TAP amplifies the light pulse. The input currents to both sections can be individually controlled. The layer structure of the PA is similar to that of the master oscillator. The active region comprises two QWs.

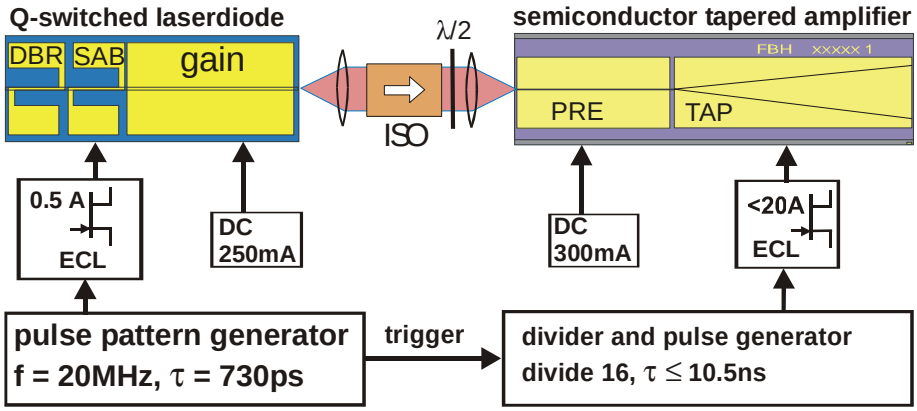

Figure 1: Scheme of the experimental setup showing the optical coupling between master oscillator and power amplifier and the electrical connections.

Whereas the PRE section is driven with a constant current (DC), the TAP is driven by a powerful ECL based electrical circuit described by Liero et al. [16]. It provides short current pulses with a peak current up to 20 A. The pulse generator HP8133A generates the necessary pulses with durations between 2 and 10.5 ns at variable repetition rates. The electrical coupling between the two pulse generators ensures a dedicated time correlation between the current pulses injected into the MO and PA and enables the possibility to adjust the delay time

between the pulses which is an important parameter determining the pulsed characteristics of the MOPA system.

The optical pulses emitted by the DBR laser are collimated with an aspheric lens with a focal length of 3.1 mm, passed through a two staged optical isolator and focused into the RW of the preamplifier of the PA with a second 3.1 mm aspheric lens.

The simulation of the propagation of the optical pulse in the PA along the *z* direction is based on a numerical solution of the travelling wave model described in [17] and [18]. The traveling wave equations for complex, slowly varying amplitudes of the forward u^+ and backward u^- propagating optical fields ($|u^+|^2+|u^-|^2$: local photon density) are coupled to the ordinary differential equations for the complex slowly varying amplitudes $p^\pm$ of the induced polarization and to the parabolic diffusion equation for real excess carrier density *N*:

$$\frac{n_g}{c_0}\partial_t u^\pm + \frac{i}{2k_0\bar{n}}\partial_{xx}u^\pm = \left(\mp\partial_z - i\beta\right)u^\pm - \frac{\bar{g}}{2}(u^\pm - p^\pm); \tag{1}$$

$$\partial_t p^\pm = \bar{\gamma}\left(u^\pm - p^\pm\right) + i\bar{\omega}p^\pm; \tag{2}$$

$$\begin{aligned}\partial_t N = D_N\partial_{xx}N + \frac{J(x,z,t)}{qd} - (AN + BN^2 + CN^3)\\ -\frac{c_0}{n_g}\mathrm{Re}\sum_{\nu=\pm}u^{\nu *}\left[gu^\nu - \bar{g}(u^\nu - p^\nu)\right].\end{aligned} \tag{3}$$

The complex propagation factor β is modeled as

$$\beta = \delta_0 - k_0\sqrt{n'N} + i\left[\frac{g'\ln(N/N_{tr})}{1+\varepsilon\|u\|^2} - \alpha\right]. \tag{4}$$

The function *J(x,z,t)* in Eq. (3) describes the injected current density, so that

$$I_{PRA} = \iint\limits_{(x,z)\in PRA} J(x,z,t)dxdz, \quad I_{TAP} = \iint\limits_{(x,z)\in TAP} J(x,z,t)dxdz$$

are the injection currents into the PRE and TAP parts of the device, respectively. Whereas I_{PRA} is kept constant in time, I_{TAP} is switched on periodically only within the relatively short time intervals $[t_c, t_c+T]\ mod(T_{per})$. Here, t_c is the initial moment of the current step, *T* is the duration of this step and T_{per} is the periodicity of the current switching. In the sequel we neglect the injection current induced heating effects, since *T* is typically only a few ns and T_{per} is by a few orders larger than *T*.

The optical fields satisfy the reflecting boundary conditions at both facets of the laser, $z=0$ and

$z=L$:

$$\begin{aligned}u^+(x,0,t) &= r_0(x)u^-(x,0,t) + a(x,t),\\ u^-(x,L,t) &= r_L(x)u^+(x,L,t),\end{aligned} \tag{5}$$

where the complex function *a(x,t)* represents an optical pulse injected into the PA through the

PRE facet. In the simulations below we assume these injected pulses to be Gaussian:

$$a(x,t)=\sqrt{\left(\frac{n_g}{c_0 d}\frac{\lambda_0}{hc_0}\right)\frac{\ln 16}{\pi w_t w_x}E_{in}}\;\; e^{i\omega_{in}t}e^{-\left(t-t_p\right)^2\ln 4/w_t^2}e^{-x^2\ln 4/w_x^2}.$$

They are characterized by the temporal FWHM w_t, temporal pulse peak position t_p, lateral FWHM w_x, and pulse energy E_{in} or related pulse peak power $P_{peak}=2\sqrt{\ln 2/\pi}\;E_{in}/w_t$.

Factors q, h and c_0 used in the formulas above denote the electron charge, the Planck constant and the speed of light in vacuum, respectively. Meaning and values of all other parameters used above are given in Table 1. We should mention that we simulated amplifiers having two or three QWs. A more detailed explanation of all parameters can be found in, e.g., [18]. For the numerical solution, we discretized the model equations by a splitting scheme, where the optical diffraction and carrier diffusion along the lateral position x are resolved by means of a fast Fourier transform, while the remaining coupled hyperbolic system in z and t is integrated along the characteristics $t\pm zn_g/c_0=const$ using a finite difference method. Finally, we mention that the model has been validated by a comparison with experimental results in previous papers [18-21].

3. Pulse propagation

We begin by considering what will happen if a Gaussian input pulse is injected into the amplifier. As mentioned above, the main purpose of the PRE section is to shape the lateral pulse profile. In what follows we analyze the impact of w_x of the input pulse with some fixed w_t and E_{in} on its amplification within the PRE section. Figures 2 (a) and (b) show the lateral profiles of the field intensities at the left (z=0) and right (z=1 mm) edge of the PRE section, respectively.

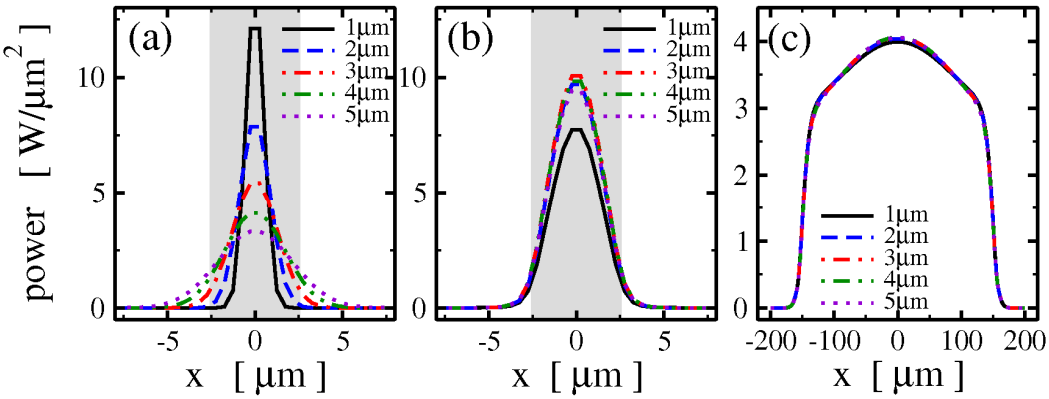

Figure 2. Lateral profiles of the normalized field intensities at (a): the left side of the PRE (z=0), (b): the right side of the PRE (z=1 mm) and (c): the right side of the TAP (z=4 mm) for different values w_x of the injected pulses. The grey shading shows the location of the narrow PRE waveguide. A 2 QW 4 mm device was simulated. The field distributions are taken at the moment t_p+Ln_g/c_0. All other parameters are as in Table 1.

One can see that independently on the initial lateral width w_x all the fields have approximately the same lateral width determined by the width of the index-guiding PRE section. We note also, that the pulses with w_x=1 μm are less amplified within the PRE, whereas w_x=3 μm is an optimal lateral width of the injected pulses. The lateral profiles of the fields emitted by the PA (panel (c)), however, are similar in all considered cases. This is due to the gain saturation at the high current injections in the TAP part of the simulated device.

Fig. 3 shows calculated snapshots of the full field distribution in the 4 mm device during the propagation of a 10 ps long Gaussian pulse (see Figure 1). The time difference between snapshots is 10 ps. In the first picture the leading edge of the injected pulse is just entering the TAP section.

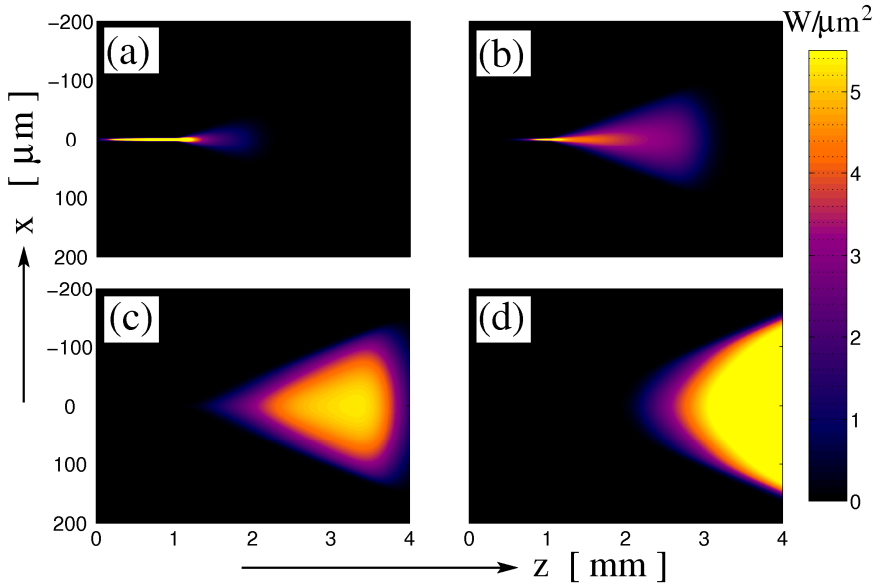

Figure 3. Simulated snapshots of the intensity distribution in the (x,z) plane of the forward propagating field in a 2 QW 4 mm long device. The injected pulse is characterized by w_t=10ps, E_{in}=10 pJ. The field distributions are taken at the moments (a): t_p+10 ps, (b): t_p+20 ps, (c): t_p+30 ps, and (d): t_p+40 ps. All other parameters are as in Table 1.

Here, large field intensity is only present within the narrow preamplifier part of the device. The next panels correspond to the later times when the leading and trailing edges of the injected pulse are travelling through the TAP. Finally, the last panel corresponds to the time when the trailing edge of the injected pulse is leaving the amplifier. Typical temporal traces of the emitted field intensity, as well as lateral profiles of the near fields and corresponding far fields at three selected time instants are shown in Fig. 4 for three input pulses of different duration w_t and energy E_{in}. Thick symbols on the pulse time traces in panel (a) indicate the time instants used to draw the near field distributions (panel (b)) and far fields (c). Black bullets in (a) as well as solid curves in (b) and (c) correspond to the time moment t_0=t_p+Ln_g/c_0, where Ln_g/c_0 is the time the pulse needs to travel through the amplifier. Thus the emitted pulse would have its peak at t_0 if the device had been transparent (i.e. no damping or amplification). The emitted pulse peak, however, occurs earlier, what can be clearly seen in the middle and lower parts of panel (a). This is due to the strong amplification of the

relatively long leading edge of the pulses. During this process the gain in the TAP is depleted, and, therefore, the amplification of the trailing edge of the pulses is less pronounced.

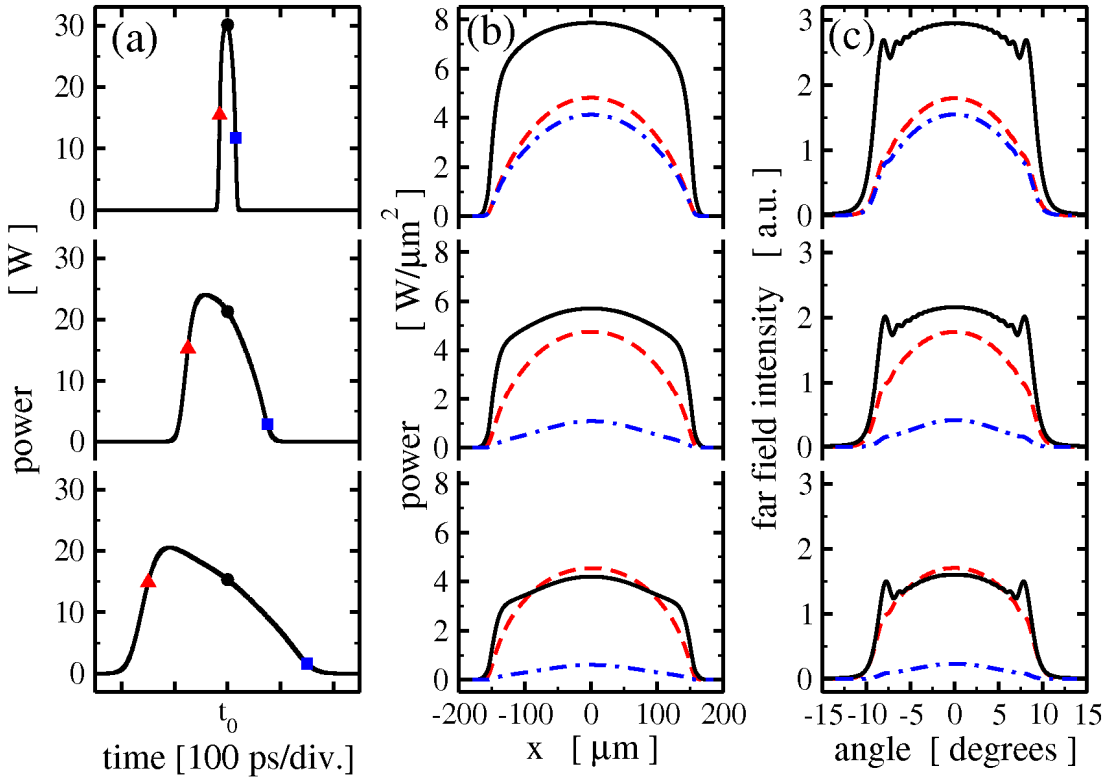

Figure 4. Representation of the optical pulses amplified in a 2 QW 4 mm device. (a): the time traces of the emitted field intensity. Thick symbols indicate three time instants t_0-t_1, t_0, and t_0+t_1. (b) and (c): the near and the far field profiles at these three time instants. From top to bottom parameters (w_t, E_{in}, t_1) are (10 ps, 10 pJ, 15 ps), (50 ps, 50 pJ, 75 ps) and (100 ps, 100 pJ, 150 ps). All other parameters are as in Table 1.

4. Comparison of theory and experiments

So far we have considered different aspects of pulse propagation through the device. In this Section we focus on a comparison of numerical and experimental results.

A typical time trace of optical pulses injected into the 2 QW 6 mm long PA is given in Fig. 5(a). The experimental pulse (black curve) is fitted by a Gaussian (red curve) with w_t=70 ps and E_{in}=60 pJ. However, the pulses in the experiments generated by the DBR laser are slightly asymmetric and have a significant trailing edge, which remains pronounced after the pulse transmission through the PA: compare theoretical and experimental curves in panel (b) of the same figure. The pulsed injection current I_{TAP} is taken to be rectangular with T=2.5 ns duration as in experiments. Fig. 5(b) shows a significant increase of output energy by a factor of 60 both in experiments and theory.

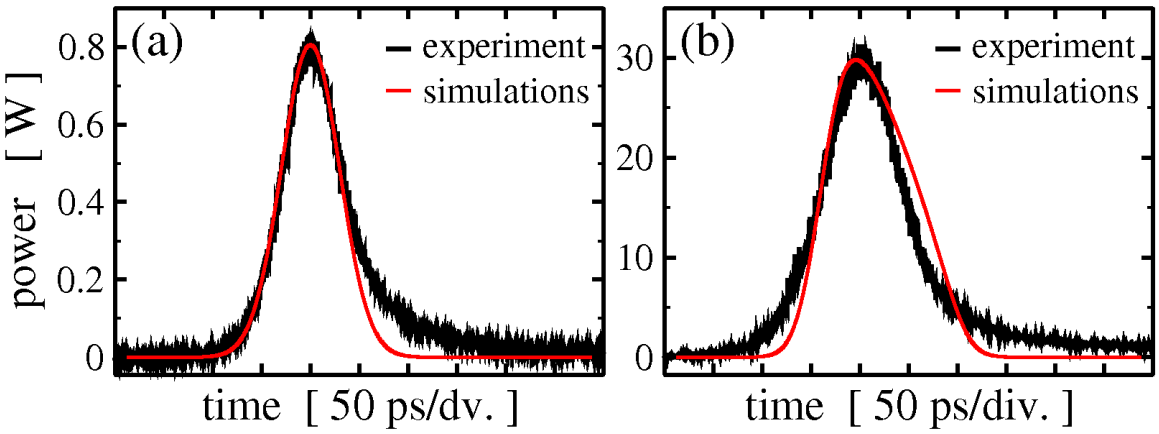

Figure 5. Measured and simulated power traces of (a): injected and (b): amplified optical pulses in a 2 QW 6 mm long optical amplifier. I_{PRE} = 13.7 mA. The other parameters are as in Table 1.

In the next step, we analyze the dependence of output energy on input energy. Fig. 6 shows an example of this dependence for a 2 QW amplifier with a length of 6 mm. The squares connected by a solid line were obtained by the numerical simulations. This Figure demonstrates that the theoretical results are in close agreement with the experimental data, which are indicated by bullets. The experimental curve reveals a slightly weaker saturation behavior than the simulated one. The discrepancy could be overcome by an adjustment of, e.g., the differential modal gain.

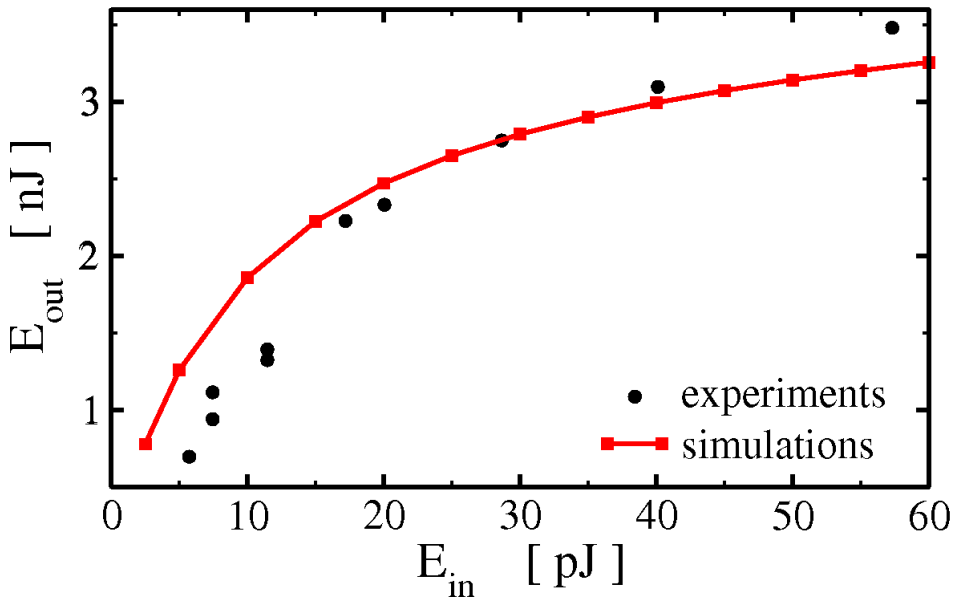

Figure 6. Comparison between the calculated (curve) and measured (bullets) dependence of the output on input energy in 2 QW 6mm long amplifier. I_{PRE} =13.7 mA. All other parameters are as in Table 1.

Next we consider the dependence of optical pulse amplification on the delay between the beginning of the bias current t_c and the injected optical pulse peak moment t_p. The results of our experiments and the numerical calculations are summarized in Fig. 7. The duration of the injection current T=10 ns while the periodicity T_{per} of the subsequent current injections was several tens or even hundreds of nanoseconds. It is apparent that when an optical pulse is injected within a time window for which the TAP remains unbiased, only some negligible pulse emission from the TAP facet is observed. Also we note that the carrier dynamics is relatively slow and once the injection current I_{TAP} is switched on the TAP section can reach the optimal amplifying conditions only after some initial time delay of 1.5-2 ns. It is clear, that optical pulses propagating through the device during this initial interval are less amplified. In the experiment, the peak power increases up to the end of the current pulse and doesn't drop to the zero immediately afterwards which could be caused by a deviation of the experimental current pulse from a rectangular shape.

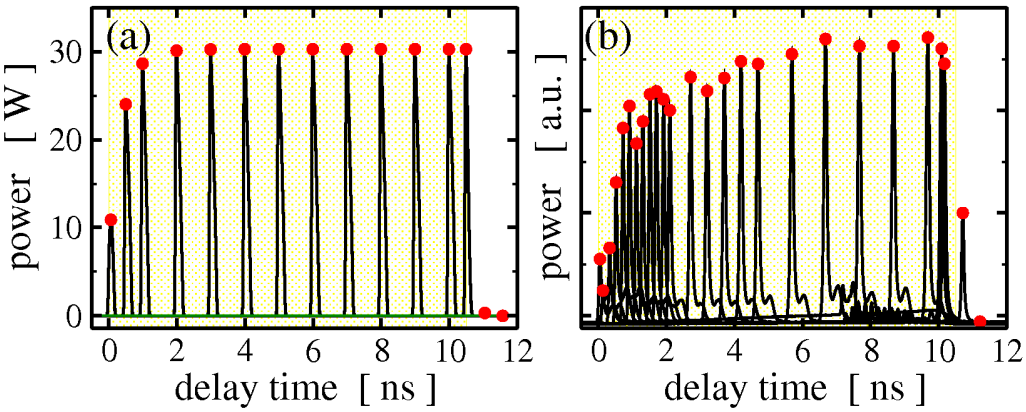

Figure 7. (a): simulations and (b): measurements of the optical pulse amplification dependence on the delay t_p-t_c of the optical pulse peak position with respect to the start of the bias current pulse. Shading: time intervals where the bias step was applied. 2 QW 6 mm long device with I_{PRE}=0.3 A and T =10 ns. The other parameters are as in Table 1.

5. Influence of material and device parameters on the pulse amplification

In this section we examine the influence of device structure and material parameters on the properties of the amplified pulses. First, in Fig. 8 we show the calculated dependence of the output energy and the maximum of the output power on the input energy of pulses for different values of the gain compression coefficient ε.

It can be seen that a decrease of gain compression coefficient leads to an increase of output energy and peak power. The simulations show a saturation of these quantities with an increase of E_{in} for all the values of gain compression coefficient considered. The value $\varepsilon = 4 \cdot 10^{-24}$ m^{-3} which is at the lower limit of the values given in [22] is the one listed in Table 1 and hence used for most of the simulations in this work because it gives the best agreement with experiment as exemplified by the results in Figs. 5 and 6. It is interesting to note that when the parameter ε approaches zero more than a hundred Watt peak power could be reached.

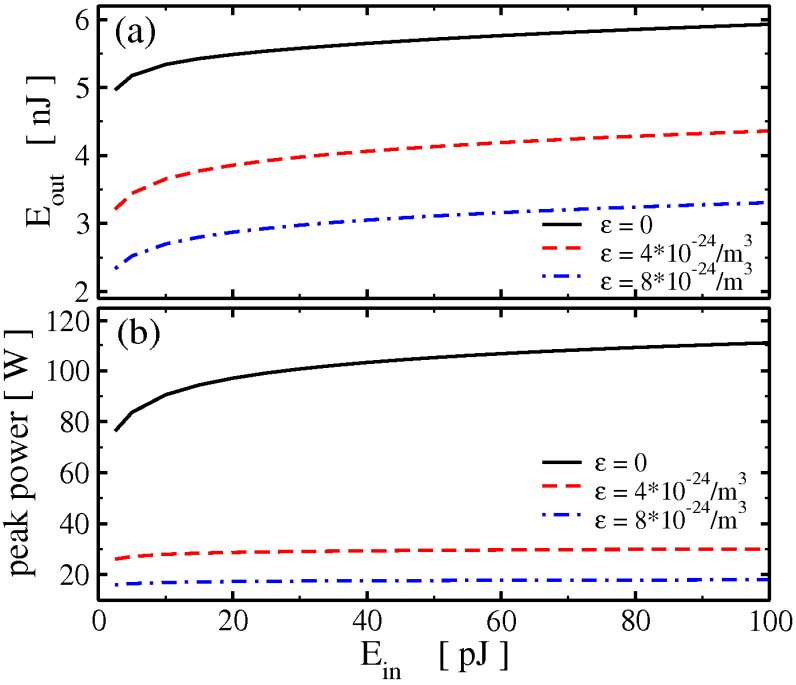

Figure 8. The dependence of (a): energy and (b): peak power of the amplified pulse on input energy for different values of the gain compression factor. A 2 QW 6mm long amplifier was considered. All other parameters are as in Table 1.

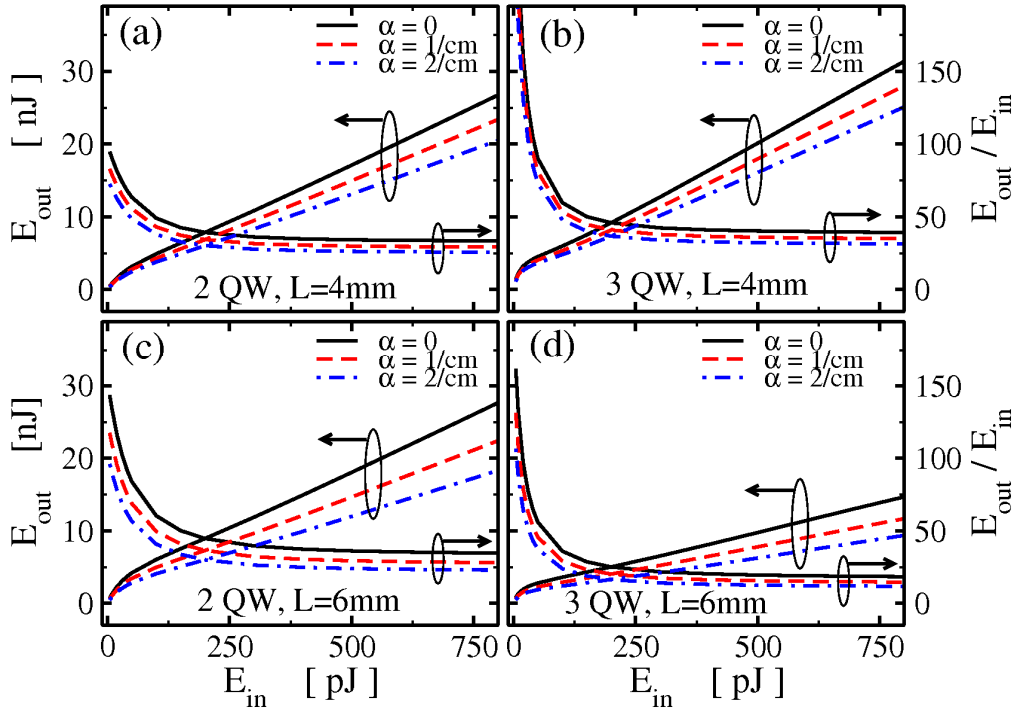

Figure 9. The dependence of output energy E_{out} and amplification factor E_{out}/E_{in} on input energy E_{in} for different loss parameter α in different simulated amplifiers. (a): 2 QW, L=4 mm. (b): 3 QW, L=4 mm. (c): 2 QW, L=6 mm. (d): 3 QW, L=6 mm. Peak power of the injected optical pulse P_{peak}=1 W, peak position t_p=3 ps. E_{in} changes in accordance to the changing pulse duration w_t. All other parameters are as in Table 1.

In Fig. 9 we present both the amplification factor (amplifier gain) E_{out}/E_{in} and the output energy as a function of input energy for 4 and 6 mm long amplifiers based on 2 or 3 quantum wells. Different lines in all panels of this figure represent different assumed loss factors α. In the presented set of simulations we have used optically injected pulses with a fixed peak power of 1 W. The energy of the input pulse is varied by tuning its temporal duration w_t. In all simulated devices we see a monotonous, nearly linear increase of the output energy with increasing input pulse energy. Moreover, in the case of 2 QW devices this growth is similar for both the 4 mm and 6 mm amplifiers. On the other hand, the amplification factor is strongly nonlinear for small and moderate energies of optical injection. We can clearly see that all considered devices are working more efficiently when amplifying injected pulses with a smaller energy. Note also, that the amplification factor of the longer 2 QW device at small energies of optical injection E_{in} is ~1.5 times higher, whereas the amplification factor is essentially the same for both 2 QW amplifiers at larger E_{in}.

In the case of 3 QW devices the situation is different. Here, the output energy and amplification factor of a shorter device are larger than those quantities in the longer amplifier. First of all we note that the injection current density in a 6 mm long device was more than 2 times smaller then such a density in a 4 mm amplifier. Since in the 3 QW device the growth of the gain function with an increase of carrier density (or current injection density) is very fast, the local gain in the long device is much smaller then in the short one. To increase the emission power and the amplification factor of the longer amplifier one should apply larger injection currents I_{TAP}.

Next, we investigate the influence of the reflectivity on the amplifier performance. In the ideal case the amplifier would have vanishing facet reflectivity r_0 and r_L, as it is assumed in most of our simulations: see Table 1. In that case an increasing bias current would cause a monotonous growth of the carrier density (i.e., the optical gain), which in turn implies a monotonous growth of the peak power and the energy of the amplified pulse. However, in reality, the device will have facets with non-vanishing reflectivity, and as a result it can behave as a resonator so that once the bias current exceeds some threshold value, the device generates light. Then instead of implying a continuing growth of the optical gain, a further increase of bias current is then transformed into a growing generated optical field power. Since the amplification of the optical pulse is directly dependent on the optical gain, we should not expect a further growth of the energy or peak power of the amplified pulse once operating with above-threshold bias currents.

Fig. 10 shows the results of calculations of devices with different reflectivity coefficients $r_0=r_L=r$. First, we note a similar amplification of the injected pulse for vanishing and small non-vanishing reflectivity: see nearly coinciding solid, dashed and dash-dotted curves around t=1 ns in all panels of Fig. 10. Next, this figure shows how an increase of reflectivity factor r implies light generation after propagation of the injected pulse. When the facet reflectivity is zero (thick solid grey curve) the device remains in a non-lasing state. However for non-vanishing reflectivity the optical gain becomes large enough to generate an optical field. A further increase of reflectivity leads to a lower value of the threshold and a clear evidence of laser operation (dashed and dash-dotted curves). The amplifier with three QWs is more prone to self-lasing than the device with two QWs, as observed experimentally, too. Note the

different reflection coefficients taken in the simulation and indicated in Fig. 10. With the termination of the current at t=3 ns, the lasing is also switched off.

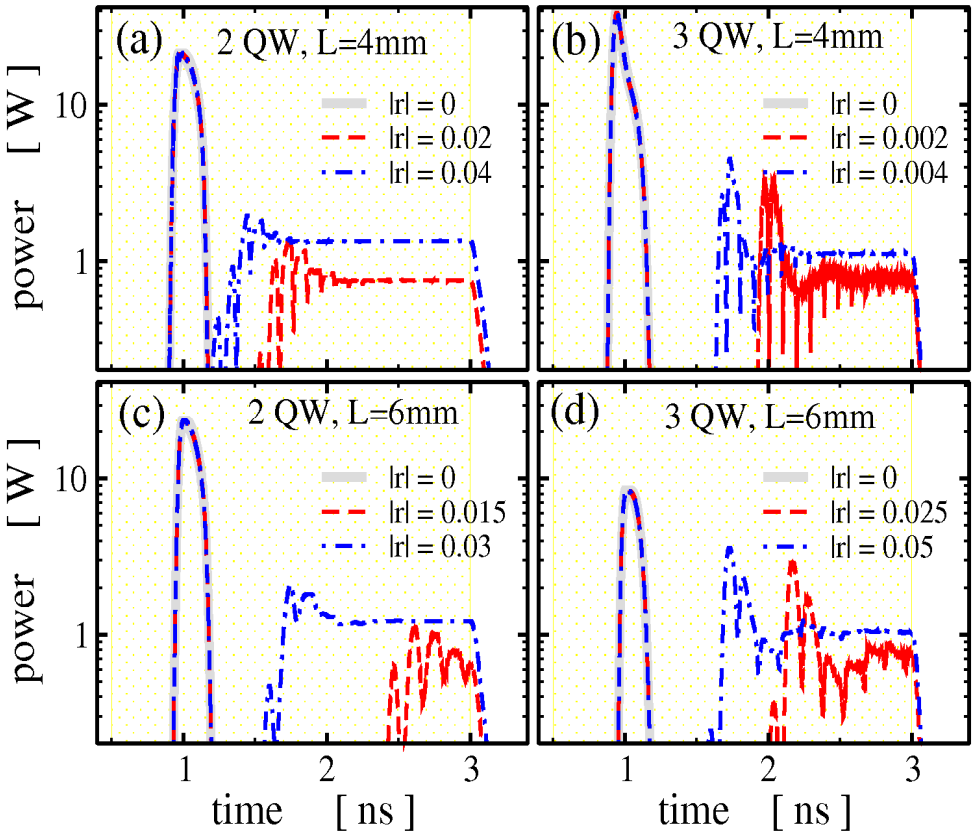

Figure 10. Pulse amplification in the devices with different reflectivity coefficients. (a): 2 QW, L=4 mm. (b): 3 QW, L=4 mm. (c): 2 QW, L=6 mm. (d): 3 QW, L=6 mm. Shading: time intervals where bias current I_{TAP} was applied. Injected optical pulse peak position t_p=1 ns. All other parameters are as in Table 1.

Finally, we discuss the impact of the carrier recombination function $(AN+BN^2+CN^3)$ to the device performance. For this reason we set the recombination parameters $B=C=0$ and tune the linear carrier relaxation time $\tau_0=A^{-1}$.

Fig. 11 shows the dependence of the output peak power (panels (a, b)) and energy (panels (b, d)) on τ_0 for devices of different lengths and number of quantum wells. In all considered cases these characteristics are monotonously increasing for increasing τ_0, i.e., for decreasing recombination parameters. This can be easily explained by reduction of the injection current needed for achieving a certain carrier density (optical gain) level. For large τ_0 the recombination function is very small and a further increase of τ_0 has no more impact to the growth of the pulse amplification. For small τ_0 the recombination function is huge, and the applied bias current can be even not sufficient to reach the transparency level, what results in vanishing peak power and energy of the propagating pulse.

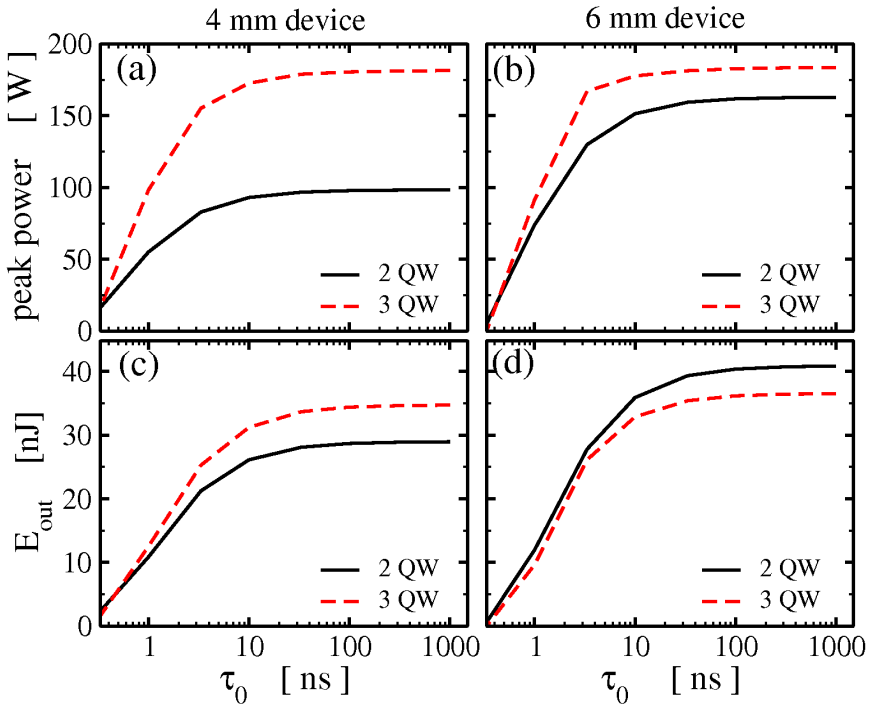

Figure 11. Output peak power (a, b) and energy (c, d) as functions of carrier life time τ_0 for 3 QW (dashed) and 2 QW (solid) devices. (a, c): 4 mm long devices. (b, d): 6 mm long devices. All other parameters are as in Table 1.

6. Conclusions

In this paper we have presented both the results of numerical simulations and experimental data for the amplification of optical pulses in devices consisting of a narrow index-guided preamplifier and a tapered power amplifier. The operation of the device has been numerically simulated using a travelling wave model. We have performed a calibration of the model parameters by fitting our simulation results to available measurements. An overall good agreement between theory and experiment has been obtained.

We have also analyzed the influence of different parameters on the amplification factor. In particular, we have studied the influence of the nonlinear gain compression factor, the non-vanishing field reflectivity of the device facets, the field absorption parameter, the carrier recombination rate, the number of quantum wells, and the length of the tapered amplifier section.

We have found that amongst the range of devices considered, the optimum performance was achieved in a 6 mm long device with two QWs. We have also found that increased field losses, carrier recombination rate, and, especially, nonlinear gain compression factor lead to a decrease of the amplified pulse peak power and energy. We have shown that non-vanishing field reflectivity at the device facets results in limitations to the growth of the optical gain and yields the light generation once the bias current exceeds a threshold value. We believe that our work provides a good basis for further research to optimize the picoseconds pulse amplification properties of the devices.

References

[1] M. Wahl, F. Koberling, M. Patting, H. Rahn, R. Erdmann, Curr. Pharm. Biotechnol. 5 (2004) 299.

[2] M. Kress, T. Meier, R. Steiner, F. Dolp, R. Erdmann, U. Ortmann, A. Rück, J. Biomed. Opt. 8 (2003) 26.

[3] M. Kuramoto, N. Kitajima, H. Guo, Y. Furushima, M. Ikeda, H. Yokoyama, Opt. Lett. 32 (2007) 2726.

[4] P. Vasilev, Ultrafast Diode Lasers—Fundamentals and Applications (Artech House, Norwood, 1995)

[5] S. Schwertfeger, A. Klehr, T. Hoffmann, A. Liero, H. Wenzel, G. Erbert, Appl. Phys. B 103 (2011) 603.

[6] M. Poelker, Appl. Phys. Lett. 67 (1995) 2762.

[7] D. Woll, J. Schumacher, A. Robertson, M.A. Tremont, R. Wallenstein, M. Katz, D. Eger, A. Englander, Opt. Lett. 27 (2002) 1055.

[8] A.J. Budz, H.K. Haugen, J. Lightware Technology 25 (2007) 3766.

[9] T. Ulm, F. Harth, H. Fuchs, J.A. L'huillier, R. Wallenstein, Appl. Phys. B, Lasers Opt. 92 (2008) 481.

[10] S. Riecke, S. Schwertfeger, K. Lauritsen, K. Paschke, R. Erdmann, G. Trankle, Appl. Phys. B, Lasers Opt. 98 (2010) 295.

[11] E. Gehrig and O. Hess, Appl. Phys. Lett. 87 (2005) 251106

[12] S.Balsamo, F.Sartori, I.Montrosset, IEEE J. Select Topics in Quantum Electron. 2 (1996) 378.

[13] B. Dagens, S. Balsamo, and I. Montrosset, IEEE J. Select Topics in Quantum Electron. 3 (1997) 233.

[14] H. Ghafouri-Shiraz, Peh Wei Tan, and T. Aruga, J. Select Topics in Quantum Electron. 3 (1997) 210.

[15] M. Premaratne, D. Nesic, G. P. Agrawal, J. Lightwave Technology 26 (2008) 1653.

[16] A. Liero, A. Klehr, S. Schwertfeger, T. Hoffmann, W. Heinrich, Proc. IMS 2010, Anaheim, USA, May 25-27 (2010) 1110.

[17] M. Lichtner and M. Spreemann, "Parallel simulation of high power semiconductor lasers," Springer Lecture Notes in Computer Science (LNCS), (2009) accepted.

[18] M. Spreemann, M. Lichtner, M. Radziunas, U. Bandelow, H. Wenzel, IEEE J. Quantum Electron., 45 (2009) 609.

[19] V.Z. Tronciu, M. Lichtner, M. Radziunas, U. Bandelow, H. Wenzel, Opt. Quantum Electron., 41 (2009) 531.

[20] C. Fiebig, V.Z. Tronciu, M. Lichtner, H. Wenzel, K. Paschke, Appl. Phys. B, 99 (2010) 209.

[21] Andreas Jechow, Mark Lichtner, Ralf Menzel, Mindaugas Radziunas, Danilo Skoczowsky, and Andrei G. Vladimirov, Optics Express 17 (2009) 19599.

[22] J. Wang, J., H. Schweizer, IEEE J. Quantum Electron 33 (1997) 1350.

Table 1 Main parameters used in simulations.

Symbol	Description	Unit	Value	
λ_0	Central wavelength	nm	1065	
n_g	Group refractive index		3.6	
α	Internal absorption	1/cm	1	
ε	Nonlinear gain compression	cm^3	$4\cdot10^{-18}$	
A	Recombination parameter	1/s	$1\cdot10^{9}$	
B	Recombination parameter	cm^3/s	$2\cdot10^{-10}$	
C	Recombination parameter	cm^6/s	$1*10^{-29}$	
D_N	Carrier diffusion coefficient	cm^2/s	25	
δ_0	Refractive index step in the trench	1/cm	-320	
	Width of the PRE	μm	5	
L_{PRE}	Length of the PRE	mm	1	
I_{PRE}	Injection current in the PRE	A	0.2	
	Full flare angle of the TAP	°	6	
L_{TAP}	Length of the TAP	mm	3 / 5	
I_{TAP}	Injection current in the TAP	A	16 / 21	
t_c	initial moment of the current step	ns	0.5	
T	typical duration of the current step	ns	2.5	
r_0	Rear facet amplitude reflectivity		0	
r_L	Front facet amplitude reflectivity		0	
w_x	Lateral FWHM of the injected pulse	μm	3	
w_t	Typical temporal FWHM of the injected pulse	ps	70	
E_{in}	Typical energy of the injected pulse	pJ	60	
t_p	Typical injected pulse peak moment	ns	2.5	
			2 QW	3 QW
g'	Differential gain	1/cm	25	61
n'	Differential index change factor	cm^3	$1.3\cdot10^{-25}$	$7.8\cdot10^{-25}$
N_{tr}	Transparency carrier density	$1/cm^3$	$1.5\cdot10^{18}$	$2\cdot10^{18}$
d	Thickness of active region	nm	14	21